Stochastic Modeling Based Variability Analysis of On-Chip Interconnects

Dries Vande Ginste[1], *Member, IEEE,* Daniël De Zutter[1], *Fellow, IEEE,* Dirk Deschrijver[2], *Member, IEEE,* Tom Dhaene[2], *Senior Member, IEEE,* Paolo Manfredi[3], *Student Member, IEEE,* Flavio Canavero[3], *Fellow, IEEE*

Abstract— In this paper, a novel stochastic modeling strategy is constructed that allows assessing parameter variability effects induced by the manufacturing process of on-chip interconnects. The strategy adopts a three-step approach. First, a very accurate electromagnetic modeling technique yields the per unit length (p.u.l.) transmission line parameters of the on-chip interconnect structures. Second, parameterized macromodels of these p.u.l. parameters are constructed. Third, a Stochastic Galerkin Method is implemented to solve the pertinent stochastic telegrapher's equations. The new methodology is illustrated with meaningful design examples, demonstrating its accuracy and efficiency. Improvements and advantages w.r.t. the state-of-the-art are clearly highlighted.

Index Terms— On-chip interconnects, variability analysis, multiconductor transmission lines, Stochastic Galerkin Method

I. INTRODUCTION

To meet the stringent design specifications, expressed in terms of speed, bandwidth, noise margin, crosstalk, etc, on-chip interconnect designers have to be aware of high-frequency phenomena. Wave effects (start to) appear on-chip, skin-effect is present, and in contrast to on-board interconnects, the semiconductors induce the so-called slow-wave effect [1]. On top of that, given the further miniaturization of the interconnects, designers have to deal with the adverse effects caused by the manufacturing process, which introduces more and more randomness. For example, the position and width of the lines are no longer deterministically known, and also, the shape of the cross-section is no longer rectangular. Due to over- or underetching or electrolytic growth, the cross-section has a random, trapezoidal shape [2]. So, designers are facing a difficult task, and to accomplish their goals they need to rely on modeling tools that accurately capture all high-frequency phenomena and allow to study variability effects.

In previous work, the influence of parameter variability effects on interconnects, and on-chip interconnects in particular, has received some attention. In [3] and [4] the influence of the cross-section was studied. Unfortunately, only a discrete set of sampling points could be considered in acceptable time. In [5] a Monte Carlo (MC) analysis of a single on-chip line was performed, clearly illustrating the importance of modeling tools that allow to study variability effects. A

brute-force MC approach [6] is, however, not tractable when dealing with multiconductor transmission lines (MTLs) in a multidimensional parameter space, as will be shown here. Compared to MC, a better stochastic modeling formalism is described in [7] and [8] where the effect of parameter uncertainty on MTLs, i.e. cables and on-board interconnects, is studied. The adopted stochastic modeling method is based on a polynomial chaos (PC) expansion with Galerkin projection, also called the Stochastic Galerkin Method (SGM) [9]–[11]. On-chip interconnect design tools would also benefit a lot from such a powerful stochastic modeling technique. It is however not straightforward to immediately extend the techniques described in [7] and [8] to on-chip interconnects, as [7] and [8] rely on basic numerical or heuristic models for the per unit length (p.u.l.) transmission line parameters of the interconnect structures. In case of on-chip interconnects, and in particular in the presence of semiconductors, accurate models are not readily available.

In this paper, a stochastic modeling strategy for on-chip interconnects is constructed, allowing to rapidly assess parameter variability effects. This is made possible by a three-step approach. First, a two-dimensional (2-D) electromagnetic modeling (EM) technique leads to a very accurate computation of the p.u.l. parameters of the on-chip MTLs. Second, using a combination of Vector Fitting (VF) [12]–[14] and barycentric Lagrange interpolation [15] multivariate parameterized macromodels of the p.u.l. parameters are constructed [16]. Third, thanks to this macromodeling step, an efficient SGM can be implemented. At this point we want to underline the benefits and novelty of this strategy w.r.t. the state-of-the-art, and in particular w.r.t. [7] and [8]. The novelty is twofold: (i) For the first time in literature, a variability analysis of *on-chip* interconnects, described as MTLs, is presented. It is clear that this application is of great importance to the community, as these interconnects are greatly affected by their manufacturing process. Using the method presented in [7] and [8], as indicated above, only cable and on-board interconnects can be dealt with; (ii) Also in contrast to what is presented in [7] and [8], and again thanks to the construction of the macromodels, the PC expansion of the p.u.l. parameters does not introduce any additional error, leading to a stochastic modeling technique with controllable accuracy, whilst being very efficient in terms of CPU time. Additionally, and for the first time, a compact formalism for the SGM for general MTLs with an arbitrary number of random stochastic parameters is presented in the appendix, allowing the readers to easily implement the method and to tailor it to their own needs (on-

[1] Electromagnetics Group, Department of Information Technology, Ghent University, Sint-Pietersnieuwstraat 41, 9000 B-Gent, Belgium. E-mail: dries.vandeginste@UGent.be, Tel.: +32 9 264 33 54, Fax: +32 9 264 99 69.
[2] Surrogate Modeling (SUMO) lab, Department of Information Technology, Ghent University-IBBT, Gaston Crommenlaan 8, 9050 B-Gent, Belgium
[3] EMC Group, Dipartimento di Elettronica, Politecnico di Torino, Corso Duca degli Abruzzi 24, 10129 Torino, Italy.

board, on-chip, etc).

This paper is organized as follows. First, in Section II some typical state-of-the-art on-chip interconnect examples are presented, for which a variability analysis is becoming imperative. Next, the stochastic modeling strategy is described in Section III for the case of a single line with one stochastic parameter. An extension to general MTLs with more than one stochastic parameter is provided in Appendix A-I. In Section IV, a variability analysis is performed for the examples presented in Section II, demonstrating excellent accuracy compared to a brute-force MC approach, and largely outperforming it in terms of CPU time. Conclusions are summarized in Section V.

II. APPLICATION EXAMPLES

(a) Single IEM line
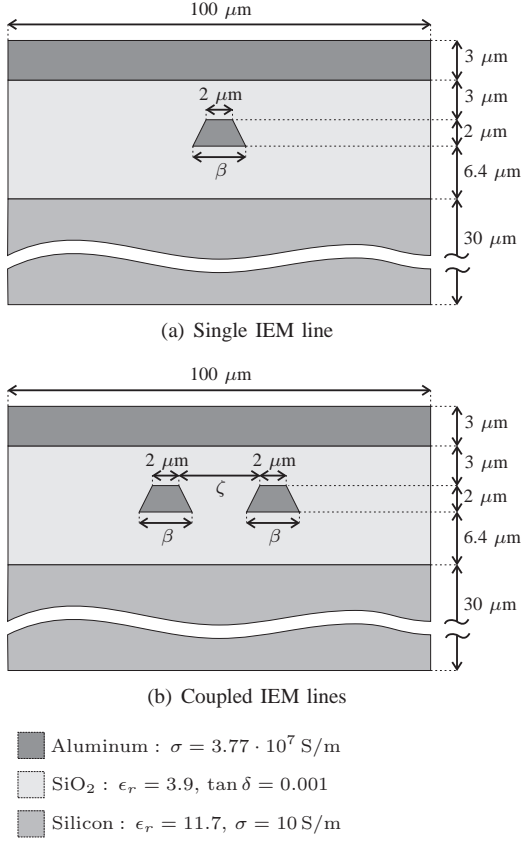

(b) Coupled IEM lines

Fig. 1: Cross-section of the IEM lines (not on scale).

There exist a large number of on-chip interconnect topologies, e.g., microstrip, co-planar waveguide, stripline. Here, we consider Inverted Embedded Microstrip (IEM) lines, such as the ones presented in Fig. 1. The IEM gains importance in high-frequency IC-design [17], because it combines the advantages of classic microstrips (well-known modeling, smaller on-chip area needed than co-planar waveguide topology, etc) with the availability of a nearly ideal (non-broken) ground plate. Of course, the stochastic modeling strategy presented in Section III is applicable to any on-chip interconnect topology.

The particular IEM topology of Fig. 1 comprises a doped Silicon substrate with a thickness of 30 μm, a relative permittivity $\epsilon_r = 11.7$, and a conductivity $\sigma = 10$ S/m on

which an insulator is placed. This insulator is 11.4 μm thick SiO$_2$ with a relative permittivity $\epsilon_r = 3.9$ and a loss tangent $\tan\delta = 0.001$. On top of the SiO$_2$ the top-plate ground is found. This ground plate has a thickness of 3 μm and is Aluminum with a conductivity $\sigma = 3.77 \cdot 10^7$ S/m. The Aluminum interconnect is embedded in the SiO$_2$ at a height of 6.4 μm above the semiconductor. Due to the etching or electrolytic growth process, the cross-sections of the lines have a trapezoidal shape. This is indicated by the stochastic parameter β, i.e. the length of the bottom base of the trapezoid. Here, the height and the length of the top side of the trapezoids are fixed to 2 μm. For the pair of coupled lines of Fig. 1(b), there is a second stochastic parameter, i.e. ζ, the gap between the lines. Due to nonperfect alignment this gap is random and is considered to be independent from the parameter β.

III. STOCHASTIC MODELING STRATEGY

A three-step approach is developed to accurately and efficiently predict the effects of parameter variability. For clarity and ease of annotation, this modeling strategy is described below for the case of a *single* line (with a reference conductor) and with *one* stochastic parameter, such as the application example shown in Fig. 1(a). A general framework for MTLs with an arbitrary number of stochastic parameters is given in Appendix A-I.

A. Two-dimensional (2-D) electromagnetic (EM) modeling

Consider a uniform transmission line where the axis of invariance is the z-axis. The transmission line is composed of one signal conductor and a reference conductor and one geometrical parameter β is random. In the Laplace domain — using the complex variable $s = j2\pi f$, where f denotes the frequency — the governing telegrapher's equations, describing this transmission line's behavior, are:

$$\frac{d}{dz}V(z,s,\beta) = -Z(s,\beta)\,I(z,s,\beta), \qquad (1)$$

$$\frac{d}{dz}I(z,s,\beta) = -Y(s,\beta)\,V(z,s,\beta), \qquad (2)$$

where $V(z,s,\beta)$ and $I(z,s,\beta)$, i.e. the voltage and current along the line, are functions of the frequency and of the distance z along the lines. They also depend on the stochastic parameter β. The p.u.l. impedance and admittance parameters are denoted $Z(s,\beta)$ and $Y(s,\beta)$ respectively, and they both depend on the frequency and on the stochastic parameter. To very accurately compute these p.u.l. parameters a 2-D EM modeling technique is adopted. As this technique has already been abundantly detailed and validated in literature [18], [19], here we only repeat the gist of it.

The 2-D EM technique assumes a quasi-TM behavior of the fields. Given the small cross-section of on-chip interconnects, this is a valid assumption. A careful definition of the circuit currents, taking semiconductors into account, leads to a concise complex capacitance and a complex inductance problem formulation. By introducing a differential surface admittance operator, these two problems are cast as boundary integral equations (BIEs), which can be solved efficiently (no volume

discretized is needed) and with high precision (skin effect and slow-wave effect are accurately taken into account). Following this procedure, accurate p.u.l. parameter data for a set of frequency samples within in a very broad band, ranging from DC till 100 GHz, and for a set of samples of the parameter β is obtained. Numerical results for the p.u.l. parameters of the structures presented in Section II can be found in [4].

B. Parameterized macromodeling

Starting from this data, first, for V samples of the stochastic parameter β, denoted β_v, $v = 1, \ldots, V$, macromodels $Z^{\mathrm{umm}}(s, \beta_v)$ and $Y^{\mathrm{umm}}(s, \beta_v)$ are constructed using Vector Fitting [12]. These are univariate macromodels, i.e. they only depend on frequency. Second, as in [16], the univariate macromodels are strung together by means of barycentric Lagrange interpolation [15]. A proper choice of the barycentric weights w_v, $v = 1, \ldots, V$, yields the following bivariate macromodels:

$$Z^{\mathrm{mm}}(s, \beta) = \sum_{v=1}^{V} w_v Z^{\mathrm{umm}}(s, \beta_v) \prod_{\substack{k=1 \\ k \neq v}}^{V} (\beta - \beta_k), \quad (3)$$

$$Y^{\mathrm{mm}}(s, \beta) = \sum_{v=1}^{V} w_v Y^{\mathrm{umm}}(s, \beta_v) \prod_{\substack{k=1 \\ k \neq v}}^{V} (\beta - \beta_k). \quad (4)$$

These parameterized macromodels $Z^{\mathrm{mm}}(s, \beta)$ and $Y^{\mathrm{mm}}(s, \beta)$ are rational w.r.t. to frequency and polynomial w.r.t. the stochastic parameter β.

By making use of adaptive sampling schemes [20] in the construction of the macromodels, the number of calls to the 2-D EM solver described in Section III-A is limited, reducing the CPU time. The accuracy of the macromodels (3) and (4) w.r.t. the original p.u.l. parameters $Z(s, \beta)$ and $Y(s, \beta)$ can be controlled by means of the number of poles in the Vector Fitting step and by the number of samples V. (Note that, here, the same samples β_v, $v = 1, \ldots, V$, are used for the construction of both Z^{mm} and Y^{mm}, but this is not strictly necessary.) Further computational details will be provided in Section IV.

It is important to already underline here that thanks to this macromodeling step, and in contrast to [7] and [8], an accurate and efficient stochastic modeling technique can be implemented now for on-chip interconnects, for which no empirical models of the p.u.l. parameters exist. This is theoretically described in the next sections and also numerically validated in Section IV.

C. Stochastic Galerkin Method (SGM)

In this paper, to solve the stochastic telegrapher's equations (1) and (2), an SGM is adopted, applying Galerkin projection to a Polynomial Chaos (PC) expansion of these differential equations [9], [10]. Let us assume that the stochastic parameter β is a Gaussian random variable with a mean value μ_β and a normalized standard deviation σ_β. Introducing

another Gaussian random variable ξ with zero mean and unit variance, β can be then written as

$$\beta = \mu_\beta (1 + \sigma_\beta \xi). \quad (5)$$

This assumption is not a restriction, it merely leads to a *Hermite* Polynomial Chaos (hPC) expansion (see further). Obviously, other PC expansions, for non-Gaussian distributions of β, can be constructed as well. An overview of the *generalized* PC is found in [11].

As a first step, an hPC expansion of the (macromodels of the) p.u.l. parameters is performed:

$$Z^{\mathrm{mm}}(s, \beta) = \sum_{k=0}^{K} Z_k(s) \phi_k(\xi), \quad (6)$$

$$Y^{\mathrm{mm}}(s, \beta) = \sum_{k=0}^{K} Y_k(s) \phi_k(\xi), \quad (7)$$

where $\phi_k(\xi)$ indicates the stochastic Hermite polynomial of degree k [21]. These polynomials are orthogonal w.r.t. the weighting function

$$W(\xi) = \frac{1}{\sqrt{2\pi}} e^{-\frac{1}{2}\xi^2}, \quad (8)$$

as follows:

$$< \phi_k(\xi), \phi_m(\xi) >= k! \, \delta_{km}, \quad (9)$$

where δ_{km} is the Kronecker delta and where the inner product $< f(\xi), g(\xi) >$ is defined as

$$< f(\xi), g(\xi) >= \int_{-\infty}^{+\infty} f(\xi) \, g(\xi) \, W(\xi) \, d\xi. \quad (10)$$

Hence, the expansion coefficients $Z_k(s)$ and $Y_k(s)$, $k = 0, \ldots, K$, in (6) and (7) are given by:

$$Z_k(s) = < Z^{\mathrm{mm}}(s, \beta), \phi_k(\xi) > / \, k!, \quad (11)$$

$$Y_k(s) = < Y^{\mathrm{mm}}(s, \beta), \phi_k(\xi) > / \, k!. \quad (12)$$

Second, the unknown voltage and current along the line are expanded in a similar way:

$$V(z, s, \beta) = \sum_{k=0}^{K} V_k(z, s) \phi_k(\xi), \quad (13)$$

$$I(z, s, \beta) = \sum_{k=0}^{K} I_k(z, s) \phi_k(\xi). \quad (14)$$

Third, the expansions (6), (7), (13), and (14) are substituted into the telegrapher's equations (1) and (2):

$$\frac{d}{dz} \sum_{k=0}^{K} V_k(z, s) \phi_k(\xi) = -\sum_{k=0}^{K} \sum_{l=0}^{K} Z_k(s) I_l(z, s) \phi_k(\xi) \phi_l(\xi),$$
$$(15)$$

$$\frac{d}{dz} \sum_{k=0}^{K} I_k(z, s) \phi_k(\xi) = -\sum_{k=0}^{K} \sum_{l=0}^{K} Y_k(s) V_l(z, s) \phi_k(\xi) \phi_l(\xi).$$
$$(16)$$

Fourth, a Galerkin projection is applied, meaning that (15) and (16) are weighted with the same set of $K + 1$ polynomials $\phi_m(\xi)$, $m = 0, \ldots, K$, using the inner product (10). Taking the orthogonality (9) into account, this leads to:

$$\forall m = 0, \ldots, K,$$

$$\frac{d}{dz} V_m(z, s) = -\sum_{k=0}^{K} \sum_{l=0}^{K} \alpha_{klm} Z_k(s) I_l(z, s), \qquad (17)$$

$$\frac{d}{dz} I_m(z, s) = -\sum_{k=0}^{K} \sum_{l=0}^{K} \alpha_{klm} Y_k(s) V_l(z, s), \qquad (18)$$

with

$$\alpha_{klm} = \langle \phi_k(\xi)\phi_l(\xi), \phi_m(\xi) \rangle / m!. \qquad (19)$$

Together, (17) and (18) form a matrix ordinary differential equation (ODE) in the $2(K + 1)$ unknown expansion coefficients $V_k(z, s)$ and $I_k(z, s)$, $k = 0, \ldots, K$. Thanks to the SGM, the equation does no longer depend on the stochastic parameter β.

Fifth, this ODE is solved. Thereto, pertinent boundary conditions (BCs) must be constructed. These BCs evolve from the terminations at the ends of the lines. In Appendix A-I, a framework for general BCs, also allowing stochastic variation of the terminations, is outlined in detail, together with the solution technique of general ODEs for MTLs. Here, we merely sketch the solution technique for the single line with a finite length $\mathcal{L}$, the presence of a deterministic Thévenin generator — composed of a voltage source $E_N(s)$ and an impedance $Z_N(s)$ — at the near end of the line ($z = 0$), and a deterministic load impedance $Z_F(s)$ at the far end of the line ($z = \mathcal{L}$), which leads to the following BCs:

$$V(0, s) = E_N(s) - Z_N(s) I(0, s), \qquad (20)$$

$$V(\mathcal{L}, s) = Z_F(s) I(\mathcal{L}, s). \qquad (21)$$

Application of the hPC expansion with Galerkin weighting to (20) and (21) yields a new set of $2(K + 1)$ boundary conditions, allowing to solve (17) and (18) for the $2(K + 1)$ unknown expansion coefficients $V_k(z, s)$ and $I_k(z, s)$, $k = 0, \ldots, K$. Substitution of these coefficients into (13) and (14) again, finally yields the desired voltage $V(z, s, \beta)$ and current $I(z, s, \beta)$ along the line, as a function of the stochastic parameter β. As demonstrated in Section IV, this allows to efficiently compute any desired stochastic quantity or function, such as the stochastic moments or the probability density function (PDF) of the voltage at the load, using standard analytical or numerical techniques [22].

D. Observations

Before numerically validating the proposed modeling strategy, outlined in Sections III-A, III-B, and III-C, the following three interesting observations are put forward, which can be considered as clear improvements w.r.t. the state-of-the-art:

1) An accurate variability analysis for uniform transmission lines, leveraging the SGM or any other stochastic modeling technique, can only be carried out if the p.u.l. parameters as a function of the frequency and as a function of the stochastic parameters are very accurately known (see also remark 3) below). Whereas the techniques in [7] and [8] are based on simplified models for the p.u.l. parameters of cables and on-board traces, here, the 2-D EM modeling technique of Section III-A is employed, allowing such a variability analysis of on-chip interconnects.

2) For the single line, the computation of the inner products (11) and (12) is necessary to expand the scalar p.u.l. parameters (6) and (7). In general, the computation of the expansion coefficients of the p.u.l. parameters require the weighting of these p.u.l. parameters with the proper polynomials, necessitating the evaluation of multidimensional integrals (A-8). Traditionally, numerical integration schemes, employing Gauss-Hermite cubatures [21], are required. Here, however, thanks to the macromodeling step, p.u.l. parameters are obtained that are analytically known as a function of frequency and as a function of the stochastic parameters (see (3), (4), and (A-3)). This allows efficient, closed-form integrations, drastically reducing the setup time of the SGM. This is also numerically illustrated in Section IV.

3) In standard PC techniques, expansions such as (6) and (7), can be considered as a *projection* of the p.u.l. parameters onto a vector space of polynomials. In Section III-C, this vector space $\mathcal{P}_K$ is spanned by the set of chosen polynomials ϕ_k, $k = 0, \ldots, K$, of degree at most K. Usually, such a projection introduces a loss of accuracy that is determined by the number of terms $K + 1$ used in the truncated series. Here, however, the macromodels also exhibit a polynomial behavior as a function of the stochastic parameter(s). By choosing the maximum degree $V - 1$ in (3) and (4) equal to K, the macromodels already reside in $\mathcal{P}_K$, making (6) and (7) exact! Thus, the expansion can be considered as a change of basis, rather than a projection.

The above advantages come, of course, at a cost, namely the construction of the macromodels. It is important to state that rapid multivariate parameterized macromodeling techniques [23], [24] are being developed, also allowing a controllable accuracy. Furthermore, these macromodels are computed offline and stored (CPU times are provided in Section IV). Once available, they can also be employed for any other type of PC expansion (other then *Hermite* PC), for sensitivity analysis, and for optimization purposes.

IV. VARIABILITY ANALYSIS OF IEM LINES

In this section the stochastic modeling strategy of Section III is validated and its efficiency is demonstrated, using the application examples of Section II. All computations have been performed on a Dell Precision M4500 laptop with an Intel(R) Core(TM) i7 X940 CPU running at 2.13 GHz and 8 GB of RAM.

A. Single IEM line

We consider the single IEM line shown in Fig. 1(a). The macromodels for the p.u.l. parameters are computed offline. To

obtain a relative error of 0.1%, thanks to the adaptive sampling technique, only 29 frequency samples are needed to construct the univariate macromodels $Z^{\text{umm}}(s, \beta_v)$ and $Y^{\text{umm}}(s, \beta_v)$, $v = 1, \ldots, V$, and this for $V = 4$ values of the stochastic parameter β. Hence, $29 \times 4 = 116$ calls to the 2-D EM solver are required, each sample taking 1.16 s. The macro-model building time itself takes about 6 s. So, in total, to construct $Z^{\text{mm}}(s, \beta)$ and $Y^{\text{umm}}(s, \beta)$, 140 s are needed. The results of this macromodeling step were already shown in [5], where they were used to implement a tractable MC analysis.

A variability analysis is now performed. The IEM line of Fig. 1(a) is given a finite length $\mathcal{L} = 1$ mm. It is driven by a Thévenin voltage source producing a sine wave with frequency f, amplitude $E_N(s \equiv j2\pi f)$, and with an internal impedance $Z_N = 1\,\Omega$. It is terminated by a load impedance $Z_F = (j\,2\pi f\,C_L + 1/R_L)^{-1}$, with $C_L = 1$ pF and $R_L = 1$ kΩ. To analyze the possible adverse effects of the manufacturing process, the parameter β is assumed to be a Gaussian random variable with a mean value $\mu_\beta = 2\ \mu$m and a normalized standard deviation $\sigma_\beta = 10\%$, and the SGM computation is performed. Also, as a reference, a brute-force MC analysis is carried out, using 50000 β-samples. As a result, amongst others, the output voltage $V(\mathcal{L}, s, \beta)$ at the load is computed as a function of the stochastic parameter β. In Fig. 2(a), a bode plot of the magnitude of the transfer function $H(s, \beta) = V(\mathcal{L}, s, \beta)/E(s)$ is shown, for a broad frequency band up to 100 GHz. Fig. 2(b) zooms in on the resonance around 7 GHz. The full black line indicates the mean $\mu_{|H|}$ of this output characteristic and the dashed lines show the $\pm 3\sigma_{|H|}$ deviations from this mean $\mu_{|H|}$, both computed using the novel technique. The gray lines on Fig. 2 correspond to 100 samples of the MC run; the circles (○) and squares (□) indicate the mean $\mu_{|H|}$ and the $\pm 3\sigma_{|H|}$ deviations, resp., computed using the 50000 samples of the MC run. (For clarity, the circles and squares are not shown on Fig. 2(a).) It can be observed that the novel technique and the MC run are in perfect agreement, validating the presented stochastic modeling strategy. The computation times are indicated in Table I. The setup time refers to the time that is needed in the SGM to construct the matrix ODE (17) and (18) and the corresponding boundary conditions. The solution time denotes the time needed to solve this equation for 250 frequency samples. For the technique proposed in this work, a significant speed-up factor of 32 w.r.t. the MC approach is observed. By means of a simple computation concerning the setup time, the importance of the macromodeling step can be clearly illustrated. Without the macromodels, the MC run would require 250×50000 calls to the 2-D EM solver, each one requiring 1.16 s. Hence, computing all samples would take approximately 168 days. Also the setup time for the SGM, now being only 0.02 s, would become unacceptably long. Indeed, we need to compute the coefficients $Z_k(s)$ (11) and $Y_k(s)$ (12), $k = 0, \ldots, K$. For 250 frequency samples and with $K = 3$, this requires the computation of $2 \times 250 \times 4 = 2000$ integrals of the type (10). Without the macromodels, no analytical expressions are available and these integrals need to be computed numerically, e.g., using a Gauss-Hermite cubature. When leveraging merely a five-points quadrature

rule, this already requires 10000 evaluations of the integrands, and hence, 10000 calls to the 2-D EM solver, each call taking 1.16 s. So, the setup time would become larger than three hours.

In Fig. 3 the probability density function (PDF) and the cumulative distribution function (CDF) of $|H(s, \beta)|$ for $f = 7$ GHz are shown. The full and the dashed line indicate the PDF and the CDF computed using the novel technique, the circles (○) and squares (□) are computed using the 50000 samples from the MC run. Apart from the excellent agreement, it is also observed that such results can clearly quantify the influence of the stochastic parameter β, and hence the effect of the manufacturing process on the behavior of the interconnect.
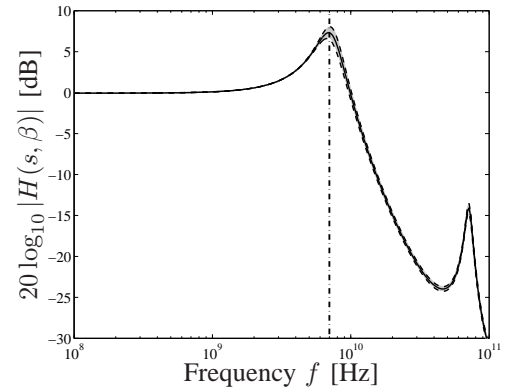
(a) Response as a function of frequency
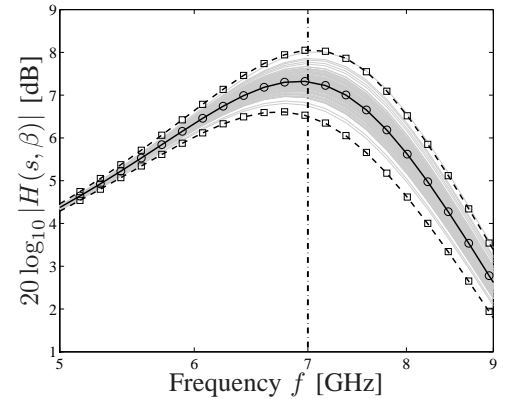
(b) Detail of Fig. 2(a) around 7 GHz, clearly illustrating the effect of the stochastic parameter β

Fig. 2: Bode plot of the magnitude of the transfer function $H(s, \beta)$ for the single IEM line. Full black line: mean $\mu_{|H|}$ computed using the novel technique; Dashed black line: $\pm 3\sigma_{|H|}$-variations computed using the novel technique; Gray lines: 100 samples from the MC run; Circles (○): mean $\mu_{|H|}$ computed using MC technique; Squares (□): $\pm 3\sigma_{|H|}$-variations computed using MC technique.

B. Coupled IEM lines

Let us now shift our attention to the pair of coupled IEM lines of Fig. 1(b). In a similar way, macromodels for the p.u.l. parameters are constructed. These are now 2×2 matrices $\overline{\mathbf{Z}}(s, \beta, \zeta)$ and $\overline{\mathbf{Y}}(s, \beta, \zeta)$, depending on the frequency

Technique	CPU time [s]			Speed-up factor
	setup	solve	total	
Novel approach	0.02	0.11	0.13	32
Monte Carlo			4.13	

TABLE I: Comparison between the efficiency of the proposed approach and an MC analysis for the single IEM line.
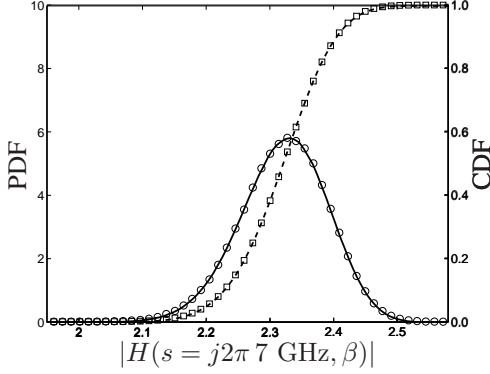

Fig. 3: PDF and CDF of the magnitude of the transfer function $H(s, \beta)$ at 7 GHz for the single IEM line. Full black line: PDF computed using the novel technique; Dashed black line: CDF computed using the novel technique; Circles ($\circ$): PDF computed using the MC technique; Squares ($\square$): CDF computed using the MC technique.

and on the two stochastic parameters β and ζ. First, univariate rational models are created using VF for a set of sampling values of the two stochastic parameters. Second, the univariate models are strung together via barycentric Lagrange interpolation. The general expressions for the multivariate macromodels can be found in Section A-I-B of the appendix. To obtain a relative error of 0.1%, the total time to construct the macromodels is about 30 minutes. This comprises 684 calls to the EM solver (19 frequency samples, 6 samples for the parameter β and 6 samples for the parameter ζ), each sample taking 2.64 s, and about 15 s for the construction of the macromodels themselves.

Consider a source-line-load configuration where the length of the two IEM lines is $\mathcal{L} = 1$ mm. The far end $z = \mathcal{L}$ of each line is terminated by a capacitive load $Z_{F,1} = Z_{F,2} = (j \, 2\pi f \, C_L + 1/R_L)^{-1}$, with $C_L = 1$ pF and $R_L = 1$ kΩ. The first line is an active line. It is driven at the near end $z = 0$ by a Thévenin voltage source producing a sine wave with frequency f, amplitude $E_{N,1}(s \equiv j2\pi f)$, and with an internal impedance $Z_{N,1} = 1\,\Omega$. The second line is the victim line. At its near end, it is terminated by a low impedance $Z_{N,2} = 1\,\Omega$. Again, a variability analysis is performed, using the novel modeling strategy and an MC run. The stochastic parameters are considered to be independent Gaussian random variables. The base β has a mean value $\mu_\beta = 2\ \mu$m and a normalized standard deviation $\sigma_\beta = 10\%$. The gap ζ has a mean value $\mu_\zeta = 3\ \mu$m and a normalized standard deviation $\sigma_\zeta = 8\%$. 250 frequency samples are calculated and for the MC run 50000 (β, ζ)-samples are used. The two output parameters that we observe here are the output voltages $V_1(\mathcal{L}, s, \beta, \zeta)$ and $V_2(\mathcal{L}, s, \beta, \zeta)$ at the loads

(a) Response as a function of frequency

(b) Detail of Fig. 4(a) around 7 GHz, clearly illustrating the effect of the stochastic parameters β and ζ
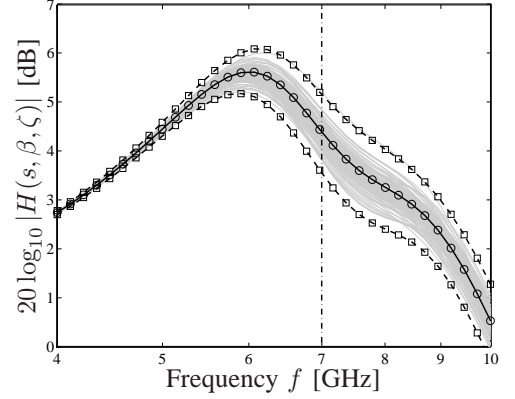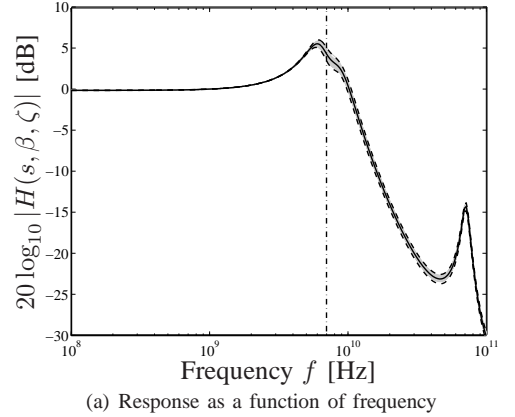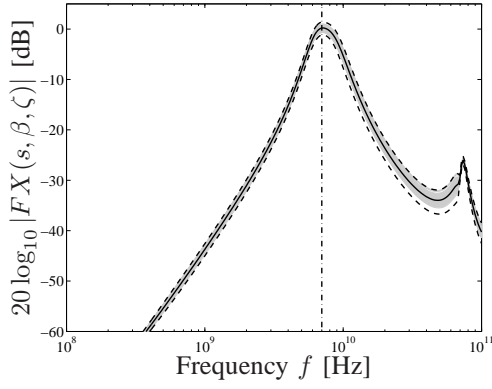
Fig. 4: Bode plot of the magnitude of the transfer function $H(s, \beta, \zeta)$ for the coupled IEM lines. The same legend as in Fig. 2 is used.

of the active and the victim line, respectively. We construct a transfer function $H(s, \beta, \zeta) = V_1(\mathcal{L}, s, \beta, \zeta)/E(s)$ and a forward crosstalk function $FX(s, \beta, \zeta) = V_2(\mathcal{L}, s, \beta, \zeta)/E(s)$. Bode plots of the magnitude of both functions are shown in Figs. 4(a) and 5(a) up to 100 GHz and magnifications of the resonance around 7 GHz are shown in Figs. 4(b) and 5(b). As before, the full black lines indicate the means $\mu_{|H|}$ and $\mu_{|FX|}$, and the dashed lines show the $\pm 3\sigma_{|H|}$ and $\pm 3\sigma_{|FX|}$ deviations from these means, all computed using the novel approach. The gray lines on the figures correspond to 100 samples of the MC run; the circles ($\circ$) and squares ($\square$) indicate the means and the $\pm 3\sigma$-deviations, resp., computed using the 50000 samples of the MC run. From Figs. 4 and 5 an excellent agreement between the MC analysis and the novel technique is observed. Comparison of CPU times between the two techniques are shown in Table II. A substantial speed-up factor of 228 is obtained. A similar reasoning as given in Section IV-A would lead again to the conclusion that the setup time without leveraging the macromodels becomes unacceptably long. The PDF and the CDF of the transfer function and of the forward crosstalk at 7 GHz are presented in Figs. 6 and 7. Apart from the excellent agreement, it is again noticed that such graphs present valuable information for designers, allowing them to rapidly assess the behavior of the interconnect.

Note that, in this paper, to make the hPC expansions of the
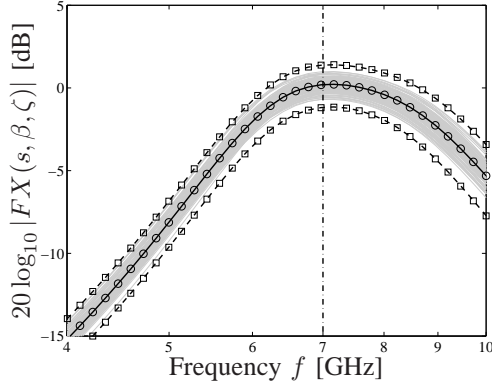
(a) Response as a function of frequency

(b) Blow-up of Fig. 4(a) around 7 GHz, clearly illustrating the effect of the stochastic parameters β and ζ

Fig. 5: Bode plot of the magnitude of the forward crosstalk $FX(s, \beta, \zeta)$ for the coupled IEM lines. The same legend as in Fig. 2 is used.

Technique	CPU time [s]			Speed-up factor
	setup	solve	total	
Novel approach	0.23	8.09	8.31	228
Monte Carlo			1895.72	

TABLE II: Comparison between the efficiency of the proposed approach and a Monte Carlo analysis for the coupled IEM lines.

p.u.l. parameters exact, as explained in Sections III and A-I, the so-called *tensor product* approach is adopted, making sure that the macromodels are elements of the pertinent vector space spanned by the Hermite polynomials. Other approaches, such as *total degree*, *hyperbolic cross*, and *Smolyak*, have also been proposed [25], limiting the number of terms in the expansions, and hence reducing both the accuracy and the computational cost. The trade-off between precision and efficiency following such schemes in the case of on-chip interconnect modeling, is a topic for further investigation.

V. CONCLUSIONS

Designers of on-chip interconnects are facing a challenging task. Due to the randomness introduced by the manufacturing process, position and widths of these lines are no longer deterministically known and their cross-sections have random trapezoidal shapes. Therefore, in this paper a novel stochastic
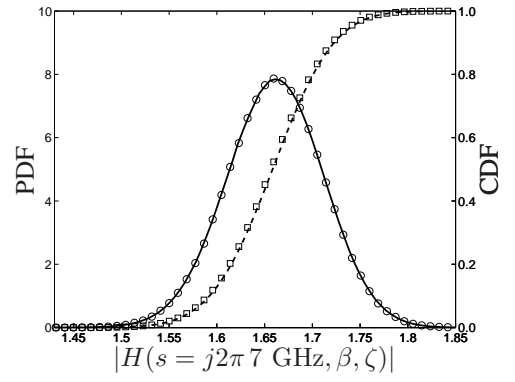

Fig. 6: PDF and CDF of the magnitude of the transfer function $H(s, \beta, \zeta)$ at 7 GHz for the pair of coupled IEM lines. The same legend as in Fig. 3 is used.
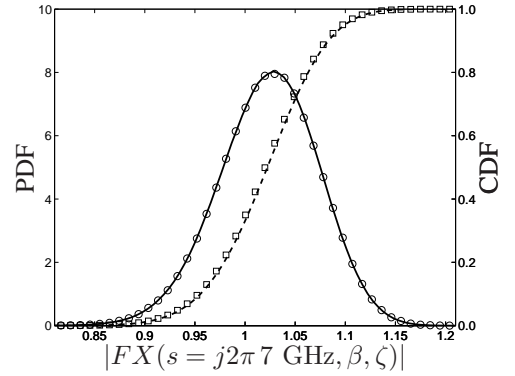

Fig. 7: PDF and CDF of the magnitude of the forward crosstalk $FX(s, \beta, \zeta)$ at 7 GHz for the pair of coupled IEM lines. The same legend as in Fig. 3 is used.

modeling strategy for the variability analysis of on-chip interconnects was presented. The strategy consists of a three-step approach. First, an accurate computation of the pertinent p.u.l. parameters using a powerful 2-D EM solver is performed. Second, parameterized macromodels of these p.u.l. parameters are constructed. These macromodels are rational as a function of frequency and polynomial as a function of the stochastic parameters. Third, a Stochastic Galerkin Method is adopted to solve the stochastic telegrapher's equations. The strategy has been applied to the variability analysis of single and coupled IEM lines. Compared to Monte Carlo runs, the novel method shows excellent agreement and superior efficiency. The improvements and advantages w.r.t. the state-of-the-art in stochastic modeling of multiconductor transmission lines were clearly outlined, the most important being that, for the first time in literature, such modeling of *on-chip* interconnects is now made possible.

In the present paper, no random variations along the z-axis were taken into account. It would however be possible to include surface roughness effects, adding to the losses along this z-direction, by incorporating a pertinent correction factor — such as the one proposed by Hammerstad and Bekkadal [26] — in the p.u.l. resistance. Extension to sensitivity and parameter variability studies of full 3-D structures, such as coupled vias in package and board plane structures [27], is currently

under investigation.

A-I. APPENDIX

In this appendix, we generalize the formulation of Section III to multiconductor transmission lines (MTL) with an arbitrary number of stochastic parameters. A technique to solve the resulting matrix ODE is also described.

A. Description of the interconnect

Consider an MTL consisting of N coupled uniform signal lines and a reference conductor. The axis of invariance is the z-axis. There are B stochastic parameters $\beta^{(b)}$, $b = 1, \ldots, B$, that influence the MTL's behavior as follows:

$$\beta^{(b)} = \mu_{\beta^{(b)}}(1 + \sigma_{\beta^{(b)}}\xi_b), \quad b = 1, \ldots, B, \qquad \text{(A-1)}$$

where ξ_b, $b = 1, \ldots, B$, are independent Gaussian random variables with zero mean and unit variance. The B-vector containing all these variable is denoted $\boldsymbol{\xi} = [\xi_1 \cdots \xi_B]^T$. The mean and normalized standard deviation of the parameters $\beta^{(b)}$ are denoted $\mu_{\beta^{(b)}}$ and $\sigma_{\beta^{(b)}}$ respectively. In the Laplace domain, using the complex variable $s = j2\pi f$, where f denotes the frequency, the telegrapher's equations, describing the MTL's behavior, are:

$$\frac{d}{dz}\left[\begin{array}{c} \mathbf{V}(z, s, \boldsymbol{\beta}) \\ \mathbf{I}(z, s, \boldsymbol{\beta}) \end{array}\right]$$
$$= -\left[\begin{array}{cc} 0 & \overline{\mathbf{Z}}(s, \boldsymbol{\beta}) \\ \overline{\mathbf{Y}}(s, \boldsymbol{\beta}) & 0 \end{array}\right] \cdot \left[\begin{array}{c} \mathbf{V}(z, s, \boldsymbol{\beta}) \\ \mathbf{I}(z, s, \boldsymbol{\beta}) \end{array}\right], \quad \text{(A-2)}$$

where the N-vectors $\mathbf{V} = [V_1 \cdots V_N]^T$ and $\mathbf{I} = [I_1 \cdots I_N]^T$ contain the voltages and currents along the N uniform coupled lines. These voltages and currents are functions of the frequency and of the distance z along the lines. They also depend on all stochastic parameters, as indicated by the set $\boldsymbol{\beta} = \{\beta^{(b)}\}_{b=1}^B$. The $N \times N$-matrices $\overline{\mathbf{Z}}(s, \boldsymbol{\beta})$ and $\overline{\mathbf{Y}}(s, \boldsymbol{\beta})$ are the p.u.l. impedance and admittance matrix, which can be computed using the 2-D EM solver described in Section III-A.

B. Parameterized macromodeling of the p.u.l. parameters

Multivariate macromodels for $\overline{\mathbf{Z}}(s, \boldsymbol{\beta})$ and $\overline{\mathbf{Y}}(s, \boldsymbol{\beta})$ are constructed. These models are rational along the dimension describing frequency and polynomial in the B other dimensions that correspond to the B stochastic parameters. So, each element of the p.u.l. impedance matrix or admittance matrix, is modeled as follows:

$$X_{ij}(s, \boldsymbol{\beta}) \approx X_{ij}^{\text{mm}}(s, \boldsymbol{\beta})$$
$$= \sum_{v^{(1)}=1}^{V^{(1)}} \cdots \sum_{v^{(B)}=1}^{V^{(B)}} w_{v^{(1)}}^{(1)} \cdots w_{v^{(B)}}^{(B)} X_{ij}^{\text{umm}}(s, \beta_{v^{(1)}}^{(1)}, \ldots, \beta_{v^{(B)}}^{(B)})$$
$$\times \prod_{\substack{k^{(1)}=1 \\ k^{(1)} \neq v^{(1)}}}^{V^{(1)}} \left(\beta^{(1)} - \beta_{k^{(1)}}^{(1)}\right) \cdots \prod_{\substack{k^{(B)}=1 \\ k^{(B)} \neq v^{(B)}}}^{V^{(B)}} \left(\beta^{(B)} - \beta_{k^{(B)}}^{(B)}\right), \qquad \text{(A-3)}$$

with $i = 1, \ldots, N$, $j = 1, \ldots, N$, and where X_{ij} stands for Z_{ij} and Y_{ij}. The univariate models X_{ij}^{umm} are rational functions of s, and are obtained through VF in a set of

sampling values $\{\beta_{v^{(1)}}^{(1)}, \ldots, \beta_{v^{(B)}}^{(B)}\}$, $v^{(b)} = 1, \ldots, V^{(b)}$, $b = 1, \ldots, B$. Hence, for each stochastic parameter $\beta^{(b)}$, $V^{(b)}$ such sampling values are used and, thus, $\prod_{b=1}^B V^{(b)}$ univariate models are required to construct the macromodels (A-3). Although it is not strictly required for the remainder of the formalism described below, here, there is opted to use the same set of sampling values for all elements of the p.u.l. matrix $\overline{\mathbf{X}}$ ($\overline{\mathbf{X}}$ stands for $\overline{\mathbf{Y}}$ and $\overline{\mathbf{Z}}$). The univariate macromodels are strung together by means of barycentric Lagrange interpolation, yielding pertinent weight coefficients $w_{v^{(b)}}^{(b)}$, $v^{(b)} = 1, \ldots, V^{(b)}$, $b = 1, \ldots, B$.

C. Stochastic Galerkin Method (SGM)

As we have considered a Gaussian distribution of the stochastic parameters, all elements of the macromodeled p.u.l. matrices are now expanded as follows:

$$X_{ij}^{\text{mm}}(s, \boldsymbol{\beta}) = \sum_{k=0}^K X_{ij,k}(s)\varphi_k(\boldsymbol{\xi}), \qquad \text{(A-4)}$$
$$i = 1, \ldots, N, \quad j = 1, \ldots, N,$$

where $\varphi_k(\boldsymbol{\xi})$ is the k-th element of a set of *multivariate* Hermite polynomials. This set is constructed by the tensor product of the B sets of univariate Hermite polynomials $\{\phi_l(\xi_b)\}_{l=0}^{V^{(b)}-1}$, $b = 1, \ldots, B$. Hence, $K = -1 + \prod_{b=1}^B V^{(b)}$, and this set of $K+1$ multivariate polynomials spans the B-dimensional vector space $\mathrm{P}_{\mathcal{V}}$ of polynomials of degree at most $\mathcal{V} = \max\{V^{(b)} - 1\}_{b=1}^B$, in which all macromodels (A-3) reside. The elements in this set are orthogonal w.r.t. the inner product

$$< f(\boldsymbol{\xi}), g(\boldsymbol{\xi}) >= \int_{\mathbb{R}^B} f(\boldsymbol{\xi})\, g(\boldsymbol{\xi})\, W(\boldsymbol{\xi})\, d\boldsymbol{\xi}, \qquad \text{(A-5)}$$

with weighting function

$$W(\boldsymbol{\xi}) = \frac{1}{\sqrt[B]{2\pi}} e^{-\frac{1}{2}\boldsymbol{\xi}^T \cdot \boldsymbol{\xi}}, \qquad \text{(A-6)}$$

as follows:

$$< \varphi_k(\boldsymbol{\xi}), \varphi_m(\boldsymbol{\xi}) >= \delta_{km} < \varphi_m(\boldsymbol{\xi}), \varphi_m(\boldsymbol{\xi}) >, \qquad \text{(A-7)}$$

where δ_{km} is the Kronecker delta. Therefore, the expansion coefficients in (A-4) are given by

$$X_{ij,k}(s) = \frac{< X_{ij}(s, \boldsymbol{\beta}), \varphi_k(\boldsymbol{\xi}) >}{< \varphi_k(\boldsymbol{\xi}), \varphi_k(\boldsymbol{\xi}) >}. \qquad \text{(A-8)}$$

Note that the expansion (A-4) is not an approximation for the macromodeled elements of the p.u.l. matrices, it is exact. Indeed, as stated above, given the polynomial interpolation (A-3), for a fixed frequency, the macromodel already resides in $\mathrm{P}_{\mathcal{V}}$, making the expansion procedure merely a change of basis. So, the barycentric Lagrange interpolation is a convenient choice that yields certain advantages, as previously discussed in Section III-D. However, this choice is not necessary. Other interpolation or approximation schemes could have been adopted during the construction of the macromodels, making the expansion (A-4) a projection onto $\mathrm{P}_{\mathcal{V}}$.

Similar as for the elements of the p.u.l. matrices, the unknown voltages and currents are now also projected onto the space $P_\mathcal{V}$:

$$V_i(z, s, \boldsymbol{\beta}) = \sum_{k=0}^{K} V_{i,k}(z, s)\varphi_k(\boldsymbol{\xi}), \qquad \text{(A-9)}$$

$$I_i(z, s, \boldsymbol{\beta}) = \sum_{k=0}^{K} I_{i,k}(z, s)\varphi_k(\boldsymbol{\xi}), \qquad \text{(A-10)}$$

$$i = 1, \ldots, N.$$

Inserting (A-4), (A-9), and (A-10) into (A-2), yields the following expressions for the $2N(K+1)$ unknown expansion coefficients $V_{i,k}$ and $I_{i,k}$, $i = 1, \ldots, N$, $k = 0, \ldots, K$, for the voltages and the currents along the MTL:

$$\frac{d}{dz} \sum_{k=0}^{K} V_{i,k}(z, s)\varphi_k(\boldsymbol{\xi})$$
$$= -\sum_{j=1}^{N}\sum_{k=0}^{K}\sum_{l=0}^{K} Z_{ij,k}(s)I_{j,l}(z, s)\varphi_k(\boldsymbol{\xi})\varphi_l(\boldsymbol{\xi}), \quad \text{(A-11)}$$

$$\frac{d}{dz} \sum_{k=0}^{K} I_{i,k}(z, s)\varphi_k(\boldsymbol{\xi})$$
$$= -\sum_{j=1}^{N}\sum_{k=0}^{K}\sum_{l=0}^{K} Y_{ij,k}(s)V_{j,l}(z, s)\varphi_k(\boldsymbol{\xi})\varphi_l(\boldsymbol{\xi}), \quad \text{(A-12)}$$

$$i = 1, \ldots, N.$$

A Galerkin projection is now adopted by weighting (A-11) and (A-12) with the same set of Hermite polynomials, using the inner product (A-5):

$$\frac{d}{dz} \sum_{k=0}^{K} V_{i,k}(z, s) < \varphi_k(\boldsymbol{\xi}), \varphi_m(\boldsymbol{\xi}) >$$
$$= -\sum_{j=1}^{N}\sum_{k=0}^{K}\sum_{l=0}^{K} Z_{ij,k}(s)I_{j,l}(z, s) < \varphi_k(\boldsymbol{\xi})\varphi_l(\boldsymbol{\xi}), \varphi_m(\boldsymbol{\xi}) >,$$
$$\text{(A-13)}$$

$$\frac{d}{dz} \sum_{k=0}^{K} I_{i,k}(z, s) < \varphi_k(\boldsymbol{\xi}), \varphi_m(\boldsymbol{\xi}) >$$
$$= -\sum_{j=1}^{N}\sum_{k=0}^{K}\sum_{l=0}^{K} Y_{ij,k}(s)V_{j,l}(z, s) < \varphi_k(\boldsymbol{\xi})\varphi_l(\boldsymbol{\xi}), \varphi_m(\boldsymbol{\xi}) >,$$
$$\text{(A-14)}$$

$$i = 1, \ldots, N, \ m = 0, \ldots, K.$$

With (A-7) and introducing the notation

$$\tilde{Z}_{ij,ml}(s) = \sum_{k=0}^{K} Z_{ij,k}(s)\frac{< \varphi_k(\boldsymbol{\xi})\varphi_l(\boldsymbol{\xi}), \varphi_m(\boldsymbol{\xi}) >}{< \varphi_m(\boldsymbol{\xi}), \varphi_m(\boldsymbol{\xi}) >},$$
$$\text{(A-15)}$$

$$\tilde{Y}_{ij,ml}(s) = \sum_{k=0}^{K} Y_{ij,k}(s)\frac{< \varphi_k(\boldsymbol{\xi})\varphi_l(\boldsymbol{\xi}), \varphi_m(\boldsymbol{\xi}) >}{< \varphi_m(\boldsymbol{\xi}), \varphi_m(\boldsymbol{\xi}) >},$$
$$\text{(A-16)}$$

$$i = 1, \ldots, N, \ j = 1, \ldots, N, \ k = 0, \ldots, K, \ m = 0, \ldots, K,$$

(A-13) and (A-14) are recast as

$$\frac{d}{dz}V_{i,m}(z, s) = -\sum_{j=1}^{N}\sum_{l=0}^{K} \tilde{Z}_{ij,ml}(s)I_{j,l}(z, s), \qquad \text{(A-17)}$$

$$\frac{d}{dz}I_{i,m}(z, s) = -\sum_{j=1}^{N}\sum_{l=0}^{K} \tilde{Y}_{ij,ml}(s)V_{j,l}(z, s), \qquad \text{(A-18)}$$

$$i = 1, \ldots, N, \ m = 0, \ldots, K.$$

The elements (A-15) and (A-16) are now organized into new $(N(K+1) \times N(K+1))$-matrices $\tilde{\overline{\mathbf{Z}}}$ and $\tilde{\overline{\mathbf{Y}}}$, which can be considered as *augmented p.u.l. matrices*. By also properly organizing the unknown expansion coefficients in $N(K+1)$-vectors $\tilde{\mathbf{V}}$ and $\tilde{\mathbf{I}}$, an augmented version of the original telegrapher's equations (A-2) is obtained, as follows:

$$\frac{d}{dz} \left[\begin{array}{c} \tilde{\mathbf{V}}(z, s) \\ \tilde{\mathbf{I}}(z, s) \end{array} \right] = - \left[\begin{array}{cc} 0 & \tilde{\overline{\mathbf{Z}}}(s) \\ \tilde{\overline{\mathbf{Y}}}(s) & 0 \end{array} \right] \cdot \left[\begin{array}{c} \tilde{\mathbf{V}}(z, s) \\ \tilde{\mathbf{I}}(z, s) \end{array} \right].$$
$$\text{(A-19)}$$

Note that, thanks to the SGM, these new equations do no longer depend on the stochastic parameters $\boldsymbol{\beta}$. As such, (A-19) can be considered as the pertinent telegrapher's equations for a deterministic MTL consisting of $N(K+1)$ signal lines, allowing to solve them with classical methods as described next.

D. Boundary conditions (BCs)

Consider now a uniform MTL, as described in Section A-I-A, with a finite length $\mathcal{L}$. The telegrapher's equations can only be solved when proper boundary conditions (BCs) are imposed. These BCs are determined by the $2N$ terminations of the N lines, which are here, for simplicity, Thévenin voltages sources. At the near end of the lines, i.e. at $z = 0$, these Thévenin voltage sources comprise a voltage source $E_{N,i}(s, \boldsymbol{\beta})$ in series with an impedance $Z_{N,i}(s, \boldsymbol{\beta})$, $i = 1, \ldots, N$. At the far end $z = \mathcal{L}$, they comprise a voltage source $E_{F,i}(s, \boldsymbol{\beta})$ in series with an impedance $Z_{F,i}(s, \boldsymbol{\beta})$, $i = 1, \ldots, N$. So, these terminations can also be of stochastic nature, which is again indicated by their dependency on $\boldsymbol{\beta}$.

Denoting the voltages and currents at the near end of the lines with the N-vectors $\mathbf{V}_N(s, \boldsymbol{\beta}) = \mathbf{V}(z = 0, s, \boldsymbol{\beta})$ and $\mathbf{I}_N(s, \boldsymbol{\beta}) = \mathbf{I}(z = 0, s, \boldsymbol{\beta})$ respectively and similarly at the far end, $\mathbf{V}_F(s, \boldsymbol{\beta}) = \mathbf{V}(z = \mathcal{L}, s, \boldsymbol{\beta})$ and $\mathbf{I}_F(s, \boldsymbol{\beta}) = \mathbf{I}(z = \mathcal{L}, s, \boldsymbol{\beta})$, it is readily seen that the boundary conditions are

$$\mathbf{V}_N(s, \boldsymbol{\beta}) = \mathbf{E}_N(s, \boldsymbol{\beta}) - \overline{\mathbf{Z}}_N(s, \boldsymbol{\beta}) \cdot \mathbf{I}_N(s, \boldsymbol{\beta}), \qquad \text{(A-20)}$$
$$\mathbf{V}_F(s, \boldsymbol{\beta}) = \mathbf{E}_F(s, \boldsymbol{\beta}) + \overline{\mathbf{Z}}_F(s, \boldsymbol{\beta}) \cdot \mathbf{I}_F(s, \boldsymbol{\beta}), \qquad \text{(A-21)}$$

where the N-vectors $\mathbf{E}_N$ and $\mathbf{E}_F$ contain the voltage sources and where the matrices $\overline{\mathbf{Z}}_N$ and $\overline{\mathbf{Z}}_F$ are diagonal matrices, containing the impedances. Obviously, other terminations, yielding full matrices $\overline{\mathbf{Z}}_N$ and $\overline{\mathbf{Z}}_F$, are equally possible.

The hPC expansion is now also applied to the BCs (A-20) and (A-21). The voltages and impedances are projected

onto $P_\mathcal{V}$:

$$E_{X,i}(s,\boldsymbol{\beta}) = \sum_{k=0}^{K} E_{X,i,k}(s)\varphi_k(\boldsymbol{\xi}), \qquad \text{(A-22)}$$

$$Z_{X,i}(s,\boldsymbol{\beta}) = \sum_{k=0}^{K} Z_{X,i,k}(s)\varphi_k(\boldsymbol{\xi}), \qquad \text{(A-23)}$$

$$i = 1,\ldots,N,$$

where X now stands for N and F. Introducing (A-22) and (A-23) into (A-20) and (A-21) and applying Galerkin weighting again, yields the following *augmented* BCs:

$$\tilde{\mathbf{V}}_N(s) = \tilde{\mathbf{E}}_N(s) - \tilde{\bar{\mathbf{Z}}}_N(s)\tilde{\mathbf{I}}_N(s), \qquad \text{(A-24)}$$

$$\tilde{\mathbf{V}}_F(s) = \tilde{\mathbf{E}}_F(s) + \tilde{\bar{\mathbf{Z}}}_F(s)\tilde{\mathbf{I}}_F(s), \qquad \text{(A-25)}$$

where the $N(K+1)$-vectors $\tilde{\mathbf{V}}_X$, $\tilde{\mathbf{I}}_X$, and $\tilde{\mathbf{E}}_X$ (X is N and F) contain the expansion coefficients of the voltages and currents along the lines and the voltages sources, respectively. The $N(K+1) \times N(K+1)$-matrices $\tilde{\bar{\mathbf{Z}}}_X$ contain the expansion coefficients of the impedances. Similar as for the augmented telegrapher's equations (A-19), the augmented BCs (A-24) and (A-25) can be considered as the pertinent BCs of a deterministic MTL consisting of $N(K+1)$ signal lines.

E. Solution of the augmented telegrapher's equations and BCs

Given the above interpretations in terms of *augmented* equations and BCs, the set of equations (A-19), (A-24), and (A-25), can now be solved as any other set of telegrapher's equations with BCs, pertaining to a deterministic system [28]. From (A-19), it is readily seen that

$$\left[\begin{array}{c} \tilde{\mathbf{V}}_F \\ \tilde{\mathbf{I}}_F \end{array}\right] = \tilde{\bar{\mathbf{T}}} \cdot \left[\begin{array}{c} \tilde{\mathbf{V}}_N \\ \tilde{\mathbf{I}}_N \end{array}\right] \qquad \text{(A-26)}$$

where the transfer matrix $\tilde{\bar{\mathbf{T}}}$ is given by

$$\tilde{\bar{\mathbf{T}}} = \left[\begin{array}{cc} \tilde{\bar{\mathbf{T}}}_{VV} & \tilde{\bar{\mathbf{T}}}_{VI} \\ \tilde{\bar{\mathbf{T}}}_{IV} & \tilde{\bar{\mathbf{T}}}_{II} \end{array}\right] = e^{-\left[\begin{array}{cc} 0 & \tilde{\bar{\mathbf{Z}}} \\ \tilde{\bar{\mathbf{Y}}} & 0 \end{array}\right]\mathcal{L}}. \qquad \text{(A-27)}$$

The BCs (A-24) and (A-25) are combined with (A-26) into one matrix equation:

$$\left[\begin{array}{cccc} \tilde{\bar{\mathbf{T}}}_{VV} & \tilde{\bar{\mathbf{T}}}_{VI} & -\bar{\mathbf{1}} & 0 \\ \tilde{\bar{\mathbf{T}}}_{IV} & \tilde{\bar{\mathbf{T}}}_{II} & 0 & -\bar{\mathbf{1}} \\ \bar{\mathbf{1}} & \tilde{\bar{\mathbf{Z}}}_N & 0 & 0 \\ 0 & 0 & \bar{\mathbf{1}} & -\tilde{\bar{\mathbf{Z}}}_F \end{array}\right] \cdot \left[\begin{array}{c} \tilde{\mathbf{V}}_N \\ \tilde{\mathbf{I}}_N \\ \tilde{\mathbf{V}}_F \\ \tilde{\mathbf{I}}_F \end{array}\right] = \left[\begin{array}{c} 0 \\ 0 \\ \tilde{\mathbf{E}}_N \\ \tilde{\mathbf{E}}_F \end{array}\right], \qquad \text{(A-28)}$$

where $\bar{\mathbf{1}}$ is the $N(K+1) \times N(K+1)$ identity matrix.

From the matrix system (A-28) the unknown expansion coefficients $\tilde{\mathbf{V}}_N$, $\tilde{\mathbf{I}}_N$, $\tilde{\mathbf{V}}_F$, and $\tilde{\mathbf{I}}_F$ can be determined using direct or iterative schemes [29]. Substitution of these coefficients into (A-9) and (A-10) for $z = 0$ and $z = \mathcal{L}$ finally yields the voltages and currents at the $2N$ terminals of the MTL as a function of frequency and as a function of the stochastic parameters $\boldsymbol{\beta}$. Using standard analytical or numerical techniques [22], any desired stochastic quantity or function, such as moments or PDFs, can now be computed.

References

[1] W. Kim and M. Swaminathan, "Characterization of co-planar silicon transmission lines with and without slow-wave effect," *IEEE Trans. on Advanced Packaging*, vol. 30, no. 3, pp. 526–532, Aug. 2007.

[2] F.-L. Lin and R.-B. Wu, "Analysis of coplanar-waveguide discontinuities with finite-metallization thickness and nonrectangular edge profile," *IEEE Trans. Microw. Theory Tech.*, vol. 45, no. 12, pp. 2131–2137, Dec. 1997.

[3] T. Demeester, D. Vande Ginste, and D. De Zutter, "Accurate study of the electromagnetic and circuit behavior of finite conducting wedges and interconnects with arbitrary cross-sections," in *Proc. of 19th IEEE Int. Conf. on Electrical Performance of Electronic Packaging and Systems (EPEPS)*, Austin, TX, USA, 24 - 27 Oct. 2010, pp. 133–136.

[4] D. Vande Ginste and D. De Zutter, "Influence of the trapezoidal cross-section of single and coupled inverted embedded microstrip lines on signal integrity," in *Proc. of the XXX URSI General Assembly and Scientific Symposium*, Istanbul, Turkey, 13 - 20 Aug. 2011, pp. 1–4.

[5] D. Vande Ginste, D. De Zutter, D. Deschrijver, T. Dhaene, and F. Canavero, "Macromodeling based variability analysis of an inverted embedded microstrip line," in *Proc. of the 20th IEEE Int. Conf. on Electrical Performance of Electronic Packaging and Systems (EPEPS)*, San Jose, CA, USA, 23 - 26 Oct. 2011, pp. 153–156.

[6] Q. Zhang, J. J. Liou, J. McMacken, J. Thomson, and P. Layman, "Development of robust interconnect model based on design of experiments and multiobjective optimization," *IEEE Trans. Electron Devices*, vol. 48, no. 9, pp. 1885–1891, Sep. 2001.

[7] I. S. Stievano, P. Manfredi, and F. G. Canavero, "Stochastic analysis of multiconductor cables and interconnects," *IEEE Trans. Electromagn. Compat.*, vol. 53, no. 2, pp. 501–507, May 2011.

[8] ——, "Parameters variability effects on multiconductor interconnects via hermite polynomial chaos," *IEEE Trans. on Components, Packaging and Manufacturing Technology*, vol. 1, no. 8, pp. 1234–1239, Aug. 2011.

[9] R. G. Ghanen and P. D. Spanos, *Stochastic Finite Elements. A Spectral Approach*. New York, USA: Springer-Verlag, 1991.

[10] D. Xiu and G. E. Karniadakis, "The Wiener-Askey polynomial chaos for stochastic differential equations," *SIAM J. Sci. Comput.*, vol. 24, no. 2, pp. 619–644, 2002.

[11] D. Xiu, "Fast numerical methods for stochastic computations: A review," *Communications in Computational Physics*, vol. 5, no. 2-4, pp. 242–272, Feb. 2009.

[12] B. Gustavsen and A. Semlyen, "Rational approximation of frequency domain responses by vector fitting," *IEEE Trans. Power Del.*, vol. 14, no. 3, pp. 1052–1061, Jul. 1999.

[13] B. Gustavsen, "Improving the pole relocating properties of vector fitting," *IEEE Trans. Power Del.*, vol. 21, no. 3, pp. 1587–1592, Jul. 2006.

[14] D. Deschrijver, M. Mrozowski, T. Dhaene, and D. De Zutter, "Macromodeling of multiport systems using a fast implementation of the vector fitting method," *IEEE Microwave and Wireless Components Letters*, vol. 18, no. 6, pp. 383–385, Jun. 2008.

[15] J. P. Berrut and L. N. Trefethen, "Barycentric Lagrange interpolation," *SIAM Review*, vol. 46, no. 3, pp. 501–517, Sep. 2004.

[16] D. Deschrijver and T. Dhaene, "Stability and passivity enforcement of parametric macromodels in time and frequency domain," *IEEE Trans. Microw. Theory Tech.*, vol. 56, no. 11, pp. 2435–2441, Nov. 2008.

[17] W. Winkler, J. Borngräber, F. Korndörfer, and C. Scheytt, "94 GHz amplifier in SiGe technology," in *Proceedings of the 38th European Microwave Conference*, Amsterdam, the Netherlands, 2008, pp. 167–170.

[18] T. Demeester and D. De Zutter, "Quasi-TM transmission line parameters of coupled lossy lines based on the Dirichlet to Neumann boundary operator," *IEEE Trans. Microw. Theory Tech.*, vol. 56, no. 7, pp. 1649–1660, Jul. 2008.

[19] ——, "Construction of the Dirichlet to Neumann boundary operator for triangles and applications in the analysis of polygonal conductors," *IEEE Trans. Microw. Theory Tech.*, vol. 58, no. 1, pp. 116–127, Jan. 2010.

[20] G. Antonini, D. Deschrijver, and T. Dhaene, "Broadband rational macromodeling based on the adaptive frequency sampling algorithm and the partial element equivalent circuit method," *IEEE Trans. Electromagn. Compat.*, vol. 50, no. 1, pp. 128–137, Feb. 2008.

[21] M. A. Abramowitz and I. A. Stegun, *Handbook of mathematical functions*. New York: Dover Publications, Inc., 1970.

[22] A. Papoulis, *Probability, Random Variables, and Stochastic Processes*, 3rd ed. McGraw-Hill, 1991.

[23] D. Deschrijver, T. Dhaene, and D. De Zutter, "Robust parametric macromodeling using multivariate orthonormal vector fitting," *IEEE Trans. Microw. Theory Tech.*, vol. 56, no. 7, pp. 1661–1667, Jul. 2008.

[24] P. Triverio, S. Grivet-Talocia, and M. Nakhla, "A parameterized macro-modeling strategy with uniform stability test," *IEEE Trans. on Advanced Packaging*, vol. 32, no. 1, pp. 205–215, Feb. 2009.

[25] J. Bäck, F. Nobile, L. Tamellini, and R. Tempone, "Stochastic spectral Galerkin and collocation methods for PDEs with random coefficients: A numerical comparison," in *Spectral and High Order Methods for Partial Differential Equations*, ser. Lecture Notes in Computational Science and Engineering, J. S. Hesthaven and E. M. Rønquist, Eds. Springer Berlin Heidelberg, 2011, vol. 76, pp. 43–62.

[26] E. O. Hammerstad and F. Bekkadal, *Microstrip Handbook*. Univ. Trondheim, Norway, 1975.

[27] Y. Li and V. Jandhyala, "Multiparameter sensitivity analysis of multiple coupled vias in board and package structures for early design and optimization," *IEEE Trans. on Advanced Packaging*, vol. 33, no. 4, pp. 1003–1011, Nov. 2011.

[28] C. R. Paul, *Analysis of Multiconductor Transmission Lines*. John Wiley & Sons, 1994.

[29] O. Axelsson, *Iterative Solution Methods*. New York: Cambridge University Press, 1994.